Arabian Journal of Chemistry (2023) **16**, 104807

King Saud University

Arabian Journal of Chemistry

www.ksu.edu.sa
www.sciencedirect.com

ORIGINAL ARTICLE

Green synthesis and characterization of new carbothioamide complexes; cyclic voltammetry and DNA/methyl green assay supported by *silico* ways versus DNA-polymerase

Amal T. Mogharbel [a], Aisha Hossan [b], Matokah M. Abualnaja [c], Enas Aljuhani [c], Rami Pashameah [c], Salhah H. Alrefaee [d], Hana M. Abumelha [e], Nashwa M. El-Metwaly [c,f,*]

[a] *Department of Chemistry, College of Science, University of Tabuk, Tabuk, Saudi Arabia*
[b] *Department of Chemistry, Faculty of Science, King Khalid University, Abha, Saudi Arabia*
[c] *Department of Chemistry, Faculty of Applied Science, Umm Al Qura University, Makkah, Saudi Arabia*
[d] *Department of Chemistry, Faculty of Science, Taibah University, Yanbu 30799, Saudi Arabia*
[e] *Department of Chemistry, College of Science, Princess Nourah bint Abdulrahman University, P.O. Box 84428, Riyadh 11671, Saudi Arabia*
[f] *Department of Chemistry, Faculty of Science, Mansoura University, Mansoura, Egypt*

Received 18 November 2022; accepted 10 March 2023
Available online 17 March 2023

KEYWORDS

Thiosemicarbazide complexes;
DNA/methyl green assay;
Cyclic voltammetry;
DNA-polymerase;
ADME parameters

Abstract Three novel complexes with the formulae of $[Ni(L)_2(H_2O)_2]$, $[Zn(HL)_2(OAc)_2]$ and $[UO_2(L)_2].2H_2O$ were synthesized from simple thiosemicarbazide derivative. The ligand in such bis-form binds either as mononegative bidentate or neutral bindentate mode. The NS donors were the binding centers towards all central atoms inside an octahedral geometry. This geometry was supported by $^3A_{2g}\rightarrow{}^3T_{1g}(P,\upsilon_3)$ and $^3A_{2g}\rightarrow{}^3T_{1g}(F,\upsilon_2)$ transitions that assigned from the bands in UV–Vis spectrum of Ni(II) complex. All structures were optimized under DFT method by using B3LYP/6-31G (d) basis set to estimate valuable quantum data. The charges of N^{11} (-0.197790) and S^{14} (-0.067486) donors describe their sufficient nucleophilicity for coordination. Cyclic voltammograms of Ni^{+2} were studied in presence of the ligand to measure the shift in redox peak that affected by the Ni^{2+}-ligand covalency. The elevated stability constants (β_{ML}) and Gibbs free energies (ΔG) suggest the successive building to stable complex in solution. The antimicrobial screening

* Corresponding author.
E-mail address: nmmohamed@uqu.edu.sa (N.M. El-Metwaly).
Peer review under responsibility of King Saud University.

Production and hosting by Elsevier

https://doi.org/10.1016/j.arabjc.2023.104807

showed an excellent inhibition role from the ligand towards the tested bacteria. Moreover, the genotoxicity of the new compounds was assessed using DNA/ methyl green assay. The ligand exhibited the best decay for the green color results from DNA/ methyl green solution. This in *vitro* investigation was strengthened by *silico* ways among that the interaction with DNA-polymerase proteins (1bpy, 5szt and 1zqa). A drug with code number MolPort-002–822-252 has high similarity to our ligand in its binding with DNA beside a low Root Mean Square Deviation value (RMSD = 0.266). Further, the ligand interacted perfectly to DG 6(T) residue in 1bpy protein *via* H-donor bond and the scoring energy value of the docking pose was excellent (S = −6.1512 kcal/mol). The BOILED-Egg indicates the ability of the ligand to absorb in brain barrier. While, there is no ability for such compound to absorb in gastrointestinal tract. Additionally, the ligand doesn't play as a substrate of P-gp protein, which is considered favorable for protecting tissues and organisms.

1. Introduction

Functionally significant biomolecules having S-N donor sites are thiosemicarbazides compounds. These compounds have gotten several importance because of their binding methods, distinctive qualities, biological relevance, and ion-sensing abilities (Casas et al., 2000). In contrast to ligands or metal ions alone, coordinate complexes exhibited high biological activity and features (West et al., 1990). Application areas for carbothioamide-based compounds and their related metal complexes include inorganic chemistry (West et al., 1993, Hosny et al., 2018), material sciences, Langmuir films, electrochemical sensors, as well as dramatically boosting bioactivity (West et al., 1993, Hosny et al., 2018; Liberta and West, 1992, Li et al., 2017). For the treatment of infections and tumors, the industry of drugs needs novel therapeutic medications with broad range of effects with few side effects. Therefore, new sensitive compounds that specifically increase the toxicity of drugs to cancer cells must be developed. On the other hand, the action of small bioactive compounds with DNA can result in genotoxicity, which renders cancer cells inactive. This makes DNA an appealing target for antitumor medicine. Mononuclear complexes were developed by many scientists, and their actions with DNA have been investigated (Abdel-Rhman et al., 2019). DNA proteins and metal ions may attach and interact because DNA has a good electron density whereas metal ions have a low electron density (Abu-Dief et al., 2021). On other side, DNA-polymerase is widely presented enzyme in biological systems that creates complementary DNA strands from template DNA. DNA polymerases are frequently utilized for DNA changes, among that the DNA replication, mutations and other functions (Sumrra et al., 2020), due to their crucial role in preserving genomic fidelity across replication and maintenance. In contrast side, due to their extensive use in a variety of application sectors, especially the biological one as follows, complexes of Schiff base ligands have drawn a lot of attention in recent years. Using a similar ligand extracted with propane hydrazide, complexes were then isolated, the majority of which displayed bioactivity (Alkhamis et al., 2021). The Co(II) and Cd(II) complexes were created employing Schiff base ligand with 1:1 M ratio (Morgan et al., 2017). Investigations into the Ni(II) complex made from thiosemicarbazide's pharmacological effectiveness have largely shown positive results (Leovac et al., 2007). Cobalt and nickel complexes with strong antibacterial activity were made using a thiosemicarbazone derivative with varied molar ratios (Netalkar et al., 2015). The complex has a greater apoptosis efficacy, according to flow cytometric analysis used to measure the cell death brought on by the complexes (Khandar et al., 2019). Copper and nickel thiosemicarbazone complexes were synthesized, studied, and demonstrated distinct antiviral activity (Pelosi et al., 2010). Several metal ion complexes have been created from different thiosemicarbazieds *via* monobasic or dibasic acids (Miminoshvili, 2009). Hydrazide Ni (II) and Co(II) complexes demonstrated anticancer properties (Antony et al., 2013). Co(II) and Ni(II)-thiosemicarbazone complexes' anticancer properties were also verified (Pelosi, 2010). A green synthesis of copper complex was performed (Alzahrani et al., 2020) using Schiff base derivative. It's important to note that the chemistry could have a big impact on the environment, therefore scientists meticulously examined to make sure that their procedures were as risk-free as feasible. The solvent-free treatment, a green method, was used with ball milling device in several articles (Alzahrani et al., 2020; Alkhamis et al., 2022). The combination of the reagents is firstly validated by the colors created that deviate from the original materials, which happens when they are vigorously crushed in a ball mill without using solvent. After many cleanings with a suitable solvent, the purity of solid products may be assessed (Alkhamis et al., 2021; Alzahrani et al., 2020).

In this study we intended to continue in green synthesis approach for new bivalent complexes that derived from thiosemicarbazide derivative. The new complexes were deliberately analyzed by analytical and spectral tools to characterize their chemical formulae. Quantum based program was implemented to optimize the geometries of all new compounds. Cyclic voltammogram (CV) was studied for the Ni (II) ion in different conditions to examine the degree of stability of the complex formed with the ligand in solution. In *vitro*, the antimicrobial efficiency of the complexes was investigated as well as their ability to bind with DNA was tested *via* DNA/methyl green method. This application was supported by utilizing *silico* methods concerning the most effective compound (the ligand) to investigate the default biological behavior inside living cells.

2. Experimental part

2.1. Reagents

To synthesize thiosemicarbazide derivative as 2-(3,4-dihydro naphthalen-1(2H)-ylidene)-N-ethyl hydrazine-1-carbothioamide (HL), N-ethyl hydrazinecarbothioamide and 3,4-dihydronaphthalen-1(2H)-one were obtained from Sigma & Aldrich. Additionally, on the other side the three complexes were prepared from $[Ni(OAc)_2].4H_2O$, $[Zn(OAc)_2].2H_2O$ and $[UO_2(OAc)_2].2H_2O$ compounds that purchased also from Sigma & Aldrich. Glacial acetic, ethanol (EtOH) and dimethyl sulfoxide (DMSO) were used as they obtained due to their extra-pure nature. The ATCC's agency provided the microbial strains as a holding for biological products and vaccinations. Tris-buffer, $MgSO_4$, and methyl green/DNA have also been purchased from Institute Fermentation of Osaka (IFO).

2.2. Synthesis of the ligand (HL)

The HL ligand was synthesized by mixing N-ethyl hydrazine carbothioamide (0.01 mol, 1.19 g) and 3,4-dihydronaphthalen-1(2H)-one (0.01 mol,1.46 g) in EtOH (50 mL) with addition of glacial acetic acid (three drops) (Alkhamis et al., 2022). The reaction was kept under reflux for 3hr, then the reddish brown precipitate was isolated by filtration and washed by EtOH several times. The dried solid (under $CaCl_2$) was analyzed to estimate its elemental percentages in addition to other analytical data (Table 1). Notice: HL is the abbreviation of the ligand which suggested based on the labile hydrogen existed in thioamide group.

2.3. The strategy of green synthesis for the complexes

The weights of reactants applied for green synthesis of complexes were reported in Scheme 1. The molar ratio utilized was 1:1 either from the ligand or the metal ion that mixed together in ball milling technique (Scheme S1) without solvent (Alkhamis et al., 2022). Just a little amount of distilled water was added to facilitate grinding of reactants that continued up to 20 min. The TLC test confirmed that the produced solid complexes were free from reactants after a deliberate washing by distilled water which followed by EtOH. These complexes were technically analyzed to investigate their chemical and structural formulae that appeared by 1metal to 2 ligand.

2.4. Equipments of analysis

For simplicity, the majority of the analysis tools were illustrated in the supplementary file as photos, and each tool's specifications were typed beneath its photo (Schemes S2 & S3). The discussion section will also include a separate report on each technique's measuring circumstances. The two ligand' NMR spectra were recorded using Bruker WP (500 MHz) in DMSO d_6 solvent and *TMS* as an internal reference. Using JENWAY type 4070 Conductance Bridge, the electrical conductivity of the complexes was assessed for 1 mmol in DMSO solvent. Additionally, through using Johnson Matthey Magnetic Susceptibility Balance, the magnetic moments were calculated by determining the magnetic susceptibility at room temperature. By utilizing a typical procedure for complexometric titration, the Ni(II) and Zn(II) ratios were determined (Vogel, 1989). While the uranium percentage was measured gravimetrically upon complete combustion for weighted sample till reach to U_3O_8 formula which cooled and then weight.

2.5. Geometry optimization

The Materials Studio software (Modeling and Simulation Solutions for Chemicals and Materials Research and Studio, 2009), the DFT method, and the DNP basis set (Frisch et al., 2009) were all used in conjunction with the DMOL3 tool to improve the structures of most compounds and compute critical parameters. Based on GGA and PBEPBE functions, the best exchange–correlation function was identified (Hehre et al., 1986). Additionally, by using B3LYP/6-31G (d) level on the DFT theory, the MEP map was established. Unfortunately, we couldn't optimize the UO_2(II) complex due to selecting of suitable conditions is not easy to reach.

2.6. Cyclic voltammetry

Nickel acetate solution was subjected to this electro-analytical method either in absence or in existence of the coordinating ligand. The cell used is a small beaker which contains 30 mL of 0.L M KCl as a supporting electrolyte. The glassy carbon working electrode (GCWE), Ag/AgCl/KCl (saturated) is the reference electrode, and the platinum wire is an auxiliary electrode used. These electrodes were linked with a potentiostat after being dipped in KCl solution.

2.7. Biological activity

A) Antimicrobial activity screening (MIC)

In accordance with procedure shown in Part A of supporting materials, the disc diffusion method was used to calculate the minimum inhibitory concentration (MIC) for the investigated drugs against various microorganisms (Al-Hazmi et al., 2020). Gram positive (*S. aureus* & *B. subtilis*) and Gram negative (*E. coli* & *P. aeuroginosa*) bacteria as well as fungi were used to assess the ligand and its associated complexes (*C. albicans* & *A. flavus*). As is widely recognized, the term MIC was employed to identify the limiting concentration that was successful in preventing the development of both bacteria and fungus throughout the experiment. The MIC test is the first stage usually employed prior clinical studies in the field

Table 1 Elemental analysis and physical data of HL and its metal complexes.

	Compound; Empirical Formula (F.W.)	Color	M.p. °C	Yield %	% Found (Calculate)		
					C	H	M
1	HL; $C_{13}H_{17}N_3S$ 247.36	Reddish brown	125	83	64.35 (63.12)	6.79 (6.90)	–
2	$[Zn(HL)_{2(}OAc)_2]$ $ZnC_{30}H_{40}N_6S_2O_4$; 678.21	Yellowish white	190	96	53.22 (53.13)	5.97 (5.94)	9.70) (9.64)
3	$[Ni(L)_2(H_2O)_2]$ $NiC_{26}H_{36}N_6S_2O_2$; 587.43	Dark green	217	98	53.46 (53.16)	5.98 (6.18)	9.82 (9.99)
4	$[UO_2(L)_2].2H_2O$ $UC_{26}H_{36}N_6S_2O_4$; 798.76	yellow	> 300	96	39.11 (39.09)	4.51 (4.54)	29.75 (29.79)

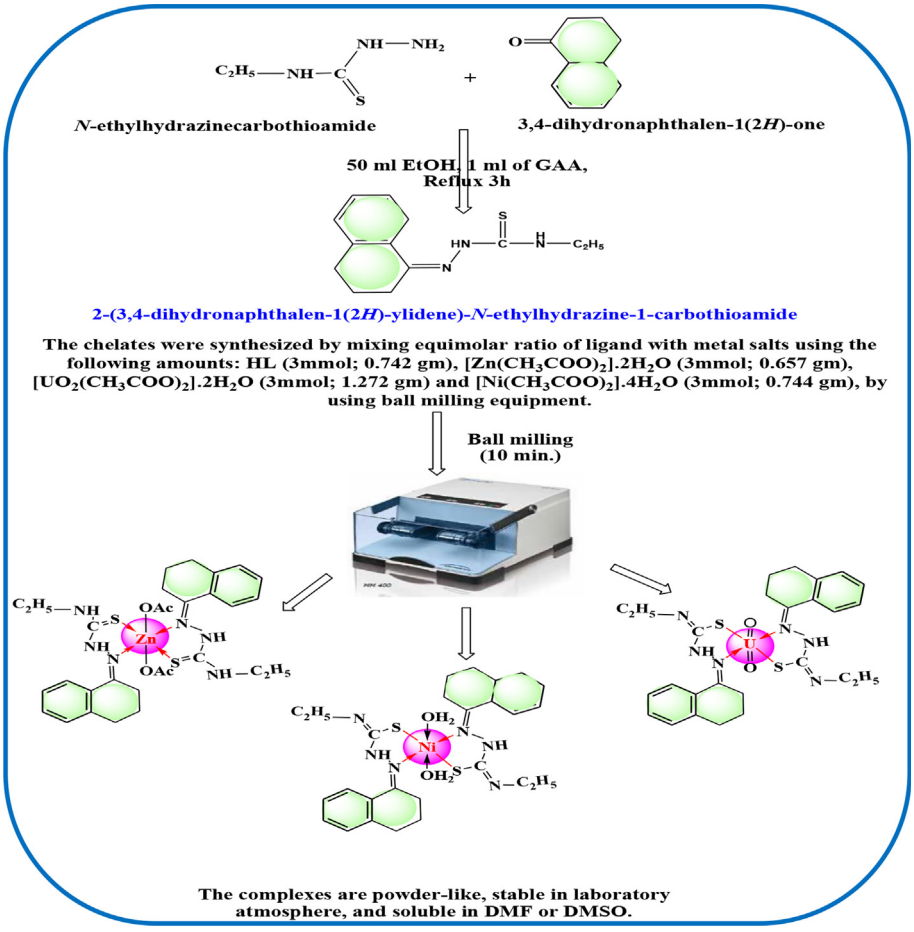

Scheme 1 The synthesis strategy y of the ligand (HL) and its metal complexes.

of medicines. It involves examining the activity of candidates against target fungi or bacteria.

B) DNA/methyl green binding test

Methyl green reacts reversibly with polymerized DNA; the molecule is stable at neutral pH, whereas the free methyl green decreased. According to the process outlined in Scheme S4 (Burres et al., 1992), the absorption of methyl green had nearly totally vanished after 24 hr in the solution of substitution reaction. Colorimetric technique was used to assess how compounds that can bind to DNA displace methyl green from the molecule. By calculating the IC_{50} value, which shows the concentration of the compound that causes the absorption to be reduced to half value, the genotoxicity of the currently used compound can be evaluated (Burres et al., 1992).

2.8. Quantum-based silico tests

This part of study aims to confirm the binding efficiency of HL ligand that appeared perfectly *invitro* assay. Various quantum-based programs were implemented for this virtual study to evaluate and to compare the biological efficiency of HL ligand. The ligand structure was optimized and saved in a suitable format to be used in docking programs (Pharmit link, MOE module & Swiss ADME). The technical details of each methodology were typed in the supporting file (Parts B and C).

3. Results and discussion

3.1. Features of molecular masses

$[Ni(L)_2(H_2O)_2]$, $[Zn(HL)_{2(}OAc)_2]$ and $[UO_2(L)_2].2H_2O$ were the formulae of the three complexes derived from thiosemicarbazide derivative (HL)(Table 1). The chemical formulae were suggested based on elemental analysis basically which supported firstly by their incomplete solubility in DMSO or DMF. Such sparingly soluble complexes must have a non-electrolytic nature. The metal (1 mol) to ligand (2 mol) ratio, 1:2, was suggested for all complexes. These bis- ligands were coordinated to complete the stable formulae beside the other secondary ligand either the acetate group or water molecules. A weighted sample (0.2 g) of each complex was kept in oven (at 70 °C) for 1 h and then cooled in dry desiccators under $CaCl_2$. The samples weight is kept constant except the UO_2(II) complex (0.191 g). This reduction in the complex weight was calculated and assigned to $2H_2O$ molecules that hydrated the coordination sphere of UO_2(II) complex. These samples were returned again to the oven (at 120 °C) for extra 1 h and after cooling they weighted. The Ni(II) complex weight (0.188 g)

was reduced in accordance with two coordinating water molecules that decomposed during heating. These observations suggested the presence of crystal water molecules with UO_2(II) complex whereas these molecules are covalently attached with nickel atom in the coordination sphere of its complex.

Further, the molecular mass of $[Zn(HL)_2(OAc)_2]$ complex (i. e.) was confirmed from its mass spectrum (Fig. 1) that performed over m/z range of 50–800, potential difference of 70 eV and heating rate of 40 °C/min. The molecular ion peak was recorded at m/z = 678.07 (calcd. 678.21) which assigns to M^+. The successive fragmentation peaks may be assigned as follow in Scheme 2. The isotopes of zinc were recorded at m/z = 66 and 67.

3.2. Analysis of IR and NMR spectra

Four absorption bands at 3242, 3309, 1049, and 1624 cm^{-1} in the IR spectrum of HL were assigned to $\upsilon(NH)_1$, $\upsilon(NH)_2$, υ(C═S), υ(C═N) vibrations, respectively (Abdel-Rhman et al., 2019; Abu-Dief et al., 2021; El-Asmy et al., 2015, Hosny et al., 2019). (Table 2, Figure S1). The profile of nuclear magnetic resonance (^{1}H NMR, DMSO d_6) (Figure S2), showed two signals at 9.80 and 10.91 ppm that were attributed to the protons of $(NH)_1$ and $(NH)_2$. Additionally, there are two signals associated to protons in the ethyl group at 2.52 ppm and 3.47 ppm. Furthermore, several signals in the range of 7.13 to 8.34 ppm signify the aromatic protons. Finally, the spectrum's

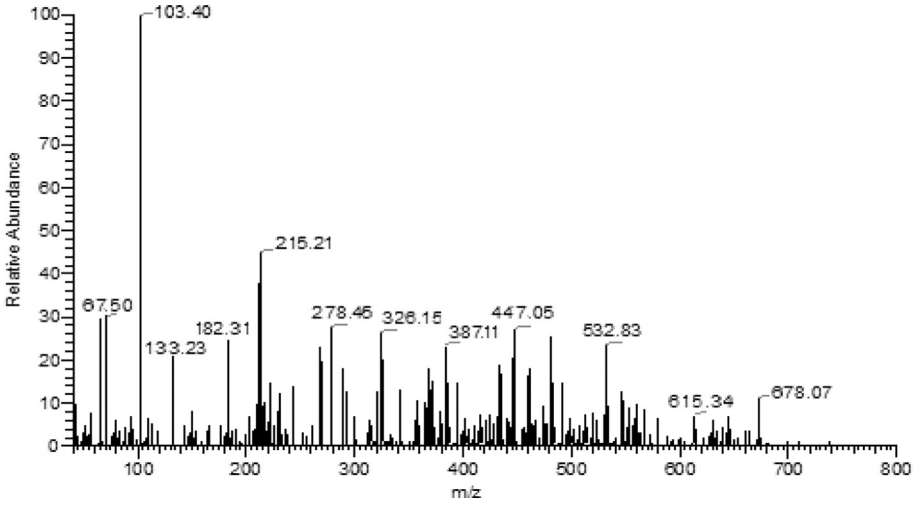

Fig. 1 The mass spectrum of $[Zn(HL)_2(OAc)_2]$ complex.

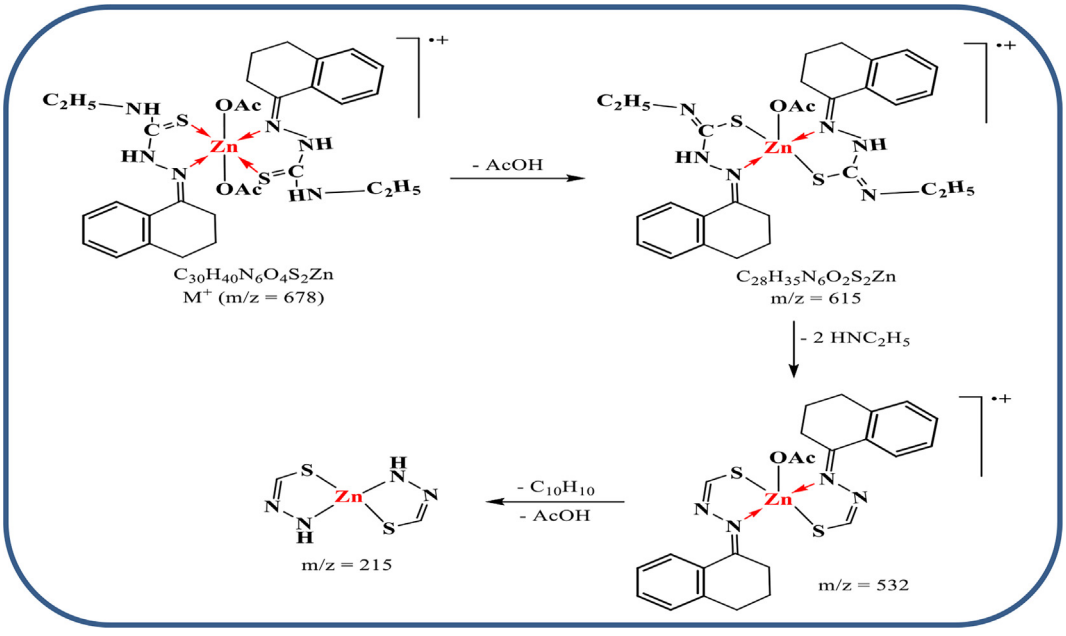

Scheme 2 Suggested fragmentation for the mass spectrum of Zn(II) complex.

Table 2 Essential IR spectral bands of HL and its metal complexes.

Compound	$\upsilon(NH)_1$	$\upsilon(NH)_2$	υ(C = N)	υ(C = S)	υ(C = N)*	υ(C-S)	υ(M−N)	υ(M−S)
1	3242	3309	1624	1049	–	–	–	–
2	3333	3377	1596	1011	1631	624	485	551
3	–	3348	1603	–	1637	613	457	502
4	–	3301	1600	–	1620	610	472	525

^{13}C NMR (Figure S3) revealed two signals at 180.06 and 168.35 ppm, respectively, that are indicative to (C═S) and (C═N). Moreover, aromatic carbons are responsible for the signals from 124.1 to 140.88 ppm range.

The IR spectra of $[Ni(L)_2(H_2O)_2]$, and $[UO_2(L)_2].2H_2O$ complexes (Figures S1) revealed a red shift of υ(C═N) vibration and disappearance of υ(C═S) and $\upsilon(NH)_1$with the instantaneous appearance of υ(C–S) bands at 610–620 and 1615–1625 cm^{-1} regions (Nakamoto, 1970). This feature suggests a mononegative bidentate mode for each coordinating ligand *via* the donors of azomethine (C═N), and deprotonated thiol (═C−S^-). The vibrations of new M−L bonds that recorded (Table 2) were assigned to υ(M−N) and υ(M−S) bands (Nakamoto, 1970). Also, $\rho_r(H_2O)$ and $\rho_w(H_2O)$ bands in the Ni(II) complex were appeared at 824 and 529 cm^{-1}, respectively. While, the broadness centered at ≈ 3300 cm^{-1}in the spectrum of UO_2(II) complex supports the presence of hydrated water molecules which already suggested (Qurban et al., 2022).

Regarding the UO_2(II) complex, the dioxouranium ion exhibited two vibrations, υ_3 & υ_1, respectively at 906 and 868 cm^{-1}. The force constant (F) of U═O bond could being estimated based on McGlynn equation (McGlynn et al., 1961) as follow; $(\upsilon_3)^2 = (1307)^2 (F_{U-O})/14.103$. The estimated F_{U-O} value (6.776 mdaynÅ^{-1}) was used to calculate the U-O bond length (R_{U-O} = 1.740 Å) from this equation; $R_{U-O} = 1.08 (F_{U-O})^{-1/3} + 1.17$. The calculated values are within the normal range of uranyl complexes (Qurban et al., 2022; McGlynn et al., 1961).

The IR spectrum of $[Zn(HL)_2(OAc)_2]$ complex (Figures S1) revealed a red shift of υ(C═N), and υ(C═S) vibrations which detects the neutral bidentate mode of bonding for each ligand. Azomethine nitrogen and thione sulfur were the coordinating atoms towards the zinc atom. This proposition was confirmed by the appearance of υ(Zn–N) and υ(Zn–S) bands at 485 and 551 cm^{-1}, respectively. Additionally, the vibrations of acetate group were appeared by a difference ($\Delta\upsilon$ > 180 cm^{-1}) refers to its mono-dentate binding nature (Nakamoto, 1970).

On the other hand the NMR spectra of Zn(II) complex were performed in DMSO d_6 (Figures S2 & S3) to elucidate the suggested structure of the complex. The ^{1}H NMR spectrum showed two signals at δ 9.89, &10.96 ppm which assignable to $(NH)_1$, and $(NH)_2$ protons, respectively. The chemical shifts are almost the same as those of the free ligand, confirming that these groups are not involved in coordination with zinc ion. Moreover, the ^{13}C NMR spectrum of the complex indicated the participation of both (C═S), and (C═N) in the coordination because they were shifted to down field.

3.3. UV–Vis spectral analysis

Electronic transitions within metal ion complexes are a good indicator for several characteristics based on the field of coordinating ligand. The transitions of intra-ligand and charge transfer are significantly affected after complexation. While, the ligand field transitions within the splitting of d-orbitals are the major indicator for the geometry of paramagnetic complexes (Lever, 1968). So, the UV–Vis spectrum of green Ni(II) complex was done for its solution in DMSO solvent along 200–1000 nm range (Al-Qahtani et al., 2021). The bands recorded at 440 and 735 nm may be assigned to $^3A_{2g}\rightarrow{}^3T_{1g}$(-P,$\upsilon_3$) and $^3A_{2g}\rightarrow{}^3T_{1g}$(F,$\upsilon_2$) transitions, respectively. These transitions are particular to the octahedral geometry of d^8 systems. The ligand field parameters as; crystal field splitting energy (**Dq** = 903), Racah parameter (**B** = 813) and nephelauetic ratio (**β** = 0.78) were calculated and found close to the known values of octahedral geometry (Lever, 1968; Al-Qahtani et al., 2021). The nephelauetic ratio reflects the high polarity of new covalent bonds formed between the metal and the ligand. Moreover, the magnetic moment value (μ_{eff} = 3.33 BM) is closer to that reported for octahedral form (Cotton et al., 2003).

3.4. Analysis of scan electron microscope (SEM) and EDX patterns

The use of accelerated beam of electrons that focused on solid samples enables to investigate the surface topography of the sample. The SEM images were obtained and displayed for investigation (Figure S4). The image of Zn(II) complex showed a uniform surface of well-spherical particulates that appeared with tiny size in micrometer range. While, the images of Ni (II) and UO_2(II) complexes exhibited a non-uniform ice-rocky shape that aggregates various spherical particles (Alkhamis et al., 2021).

The complex's Ni(II), Zn(II), or U(VI) element singlet-set of signals (Figure S5) from the EDX analysis indicate the coordination mechanism properly. For the inner layers to be penetrated in this study, accelerating x-ray photons are necessary (K- or L-shell). These photons stimulate the electrons, which subsequently produce positive gaps that readily draw other electrons from higher levels (L- or M−shell). This relaxation is coupled with radiation emitted that draw peaks of K-series (Ka1, Ka2, or Kb) or L-series. Depending on each element's distinct electronic configuration, these peaks distinguish them; the L-series being the most essential (Alkhamis et al., 2021). The wt/At% was also calculated in relation to the indicator element (heavier element as the metal).

3.5. Geometry optimizing

The geometry of HL ligand and its complexes (Figure S6) except the UO_2(II) one was optimized under DFT method. Whereas, 3D-maps (Fig. 2& S7) were demonstrated by using B3LYP/6-31G (d) basis set. These maps as well as the esti-

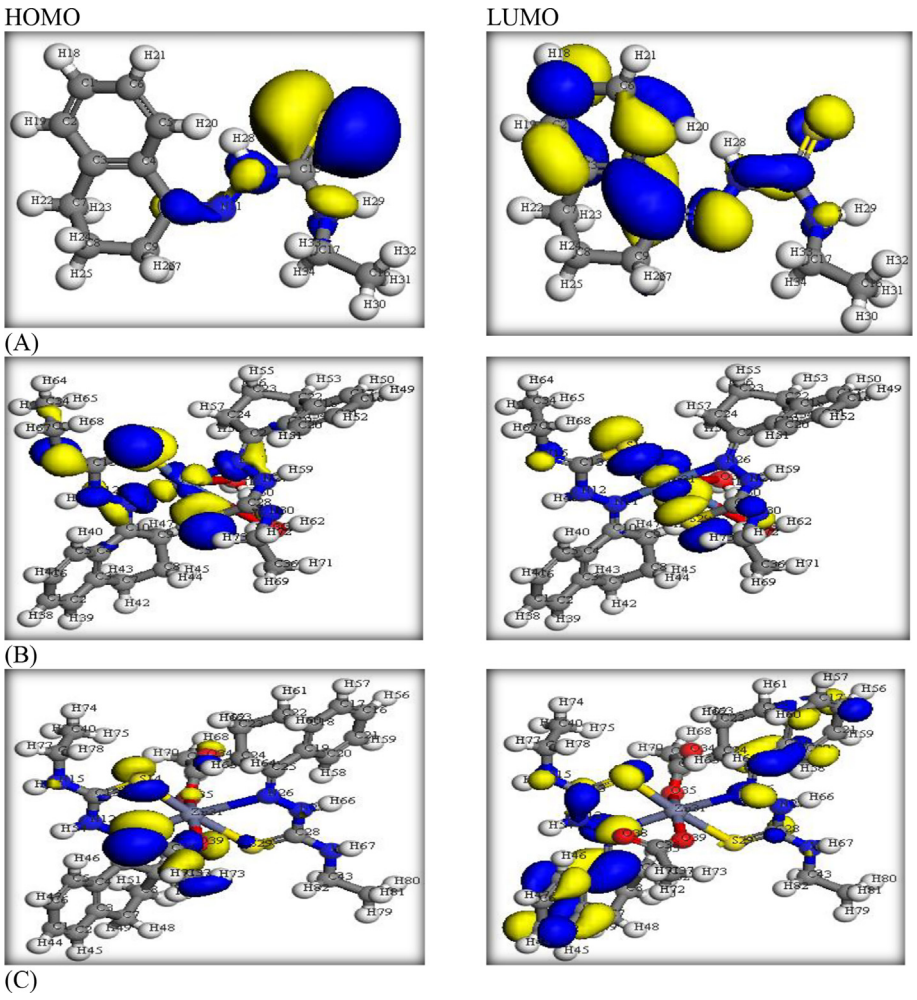

Fig. 2 HOMO & LUMO levels of (A)HL ligand, (B)Ni(II) and (C)Zn(II) complexes.

mated computational parameters (Table S1) offer a well information about the coordination process fully.

A) General features

The ligand geometry of minimum energy content (Figure S6) exhibited a suitable position of C(10) = N(11) and C(13) = S(14) groups that able to coordinate without bond strain. The charges of N^{11} (-0.197790) and S^{14} (-0.067486) donors describe their sufficient nucleophilicity for coordination with the metal ions. The bond lengths of $C^{10} = N^{11}$ (1.28182 Å) and $C^{13} = S^{14}$ (1.58265 Å) groups are significantly lengthen after the coordination of their donors (N & S) towards the metal ions (Alaysuy et al., 2022, Hosny et al., 2023). Further, the angles of S(14)-C(13)-N(12), N(12)-N(11)-C(10) and C(17)-N(15)-C(13) were 122.26°, 121.92° and 122.52°, respectively. These angles reflect the regularity of sp^2 hybridized-carbons in HL structure. While such angles were slightly shifted in the two complexes due to some normal changes happened with coordination (Figure S6).

B) 3D- models of frontier orbitals and MEP

The HOMO and LUMO patterns were demonstrated (Fig. 2) to evaluate the distribution of electron-cloud on definite functional groups. As seen, the HOMO level in HL ligand was concentrated on the functional groups that contained the donor atoms mainly, while the LUMO level was dispersed over the whole molecule (Alatawi et al., 2022). The feature of the two orbitals did not change strongly in the two complexes while they are seeming focused around the nickel center more than the zinc one. The energies of the two orbitals were computed (Table S1) and the gap between them ($\Delta E = E_{LUMO}$-E_{HOMO}) are significantly lower in the two complexes as expected.

The maps of electrostatic potential (Figure S7) were demonstrated to differentiate the nucleophilic, electrophilic, and zero-potential zones. Such zones were chromatically characterized by red, blue and green colors. As noticed in HL map, the nucleophilic zone (red) seems focused on N(11) and S(14) donors which supporting their priority in coordination among the other donors. This nucleophilicity was reduced in the two complexes depending on the coordination of these donor atoms. Further, the zero-potential zone is normally prevailing on the whole carbon skeleton.

C) Computational parameters

The energy of kinetic, binding, spin electrostatic, polarization and exchange–correlation beside the summation of atomic

energy as well as the dipole moments were estimated and tabulated (Table S1). The values of total energy, summation of atomic energy and binding energy of the two complexes are lower than the free ligand indicating the high stability of such complexes. The exchange–correlation energy and electrostatic energy values are also lowered in the complexes to confirm their priority in stability of bonds. The dipole moment of HL ligand and its corresponding complexes are relatively comparable to each other's and their values detect the reduced polarity over the whole molecules. This feature is preferable in biological application due to the ability of such compounds to miscible with cell-lipids and then may contact directly with active sites in biological systems (Abumelha et al., 2020).

3.6. Cyclic voltammetry

This study offers essential parameters that reflect a light on the changes of electrochemical behavior of nickel ion (i. e.) in presence of the ligand. This may help to understand the coordination process within the complexes in solid state as the main aim in this research. Notice: the equations implemented for this study were typed in the supporting material file (part D) to reduce the similarity in the manuscript as possible.

A) Electrochemical behavior of Ni^{2+} in absence and presence of HL at 288.55 K

The redox behavior of Ni^{2+} in 0.1 M KCl (supporting electrolyte) was studied electrochemically at 288.55 K under glassy carbon electrode (working one), potential window of 1 to −1 V and a scan rate 0.1 V/s (Fig. 3). In absence of HL ligand, the electroactivity of Ni^{2+} solution was suggested due to appearance of one cathodic and anodic peaks on the voltammogram which attributing to (Ni^{2+}/Ni^{0}) and (Ni^{0}/Ni^{2+}), respectively. The catiodic potential peak, Epc, arises to −0.4525 V in the forward scan, while the anodic potential peak, Epa, reaches to 0.0425 V in the reverse scan. The increase in all peak currents designates and supports the presence of diffusion process (Almehmadi et al., 2022). Adding HL ligand by various concentrations leads to lower shift of the redox peak due to the covalency between the Ni^{2+} ions and the ligand (Fig. 3).

B) Stability constant and Gibbs free energies for the Ni^{2+}-HL complex

Adding HL ligand to Ni^{2+} ions, the elevated stability constants (β_{ML}) and Gibbs free energies (ΔG) suggest the successive building to stable complex in solution as shown in Table 3. To calculate β_{ML} and ΔG, we must apply these Eqs. (1)–(3):

$$E^{\circ} = (E_{pa} + E_{pc})/2 \quad (1)$$

$$\Delta E^{\circ} = E^{\circ}_{C} - E^{\circ}_{M} = 2.303(RT/nF) \times (\log \beta_{ML} + j \log C_{L}) \quad (2)$$

$$\Delta G = -2.303\, RT \log \beta_{MX} \quad (3)$$

Where (EM) is the valid peak potential of the Ni^{+2} ion at zero ligand concentration, (EMl) is the valid peak potential of the complex after each addition for the ligand amount, (j = [L]/[M]) is the molar ratio, and (CL) is the molar concentration of the ligand. Finally, increasing the ligand concentration the βML and ΔG values are increased.

3.7. Invitro assays

A) Antimicrobial screening

Gram positive (*S. aureus* & *B. subtilis*), Gram negative (*E. coli* & *P. aeuroginosa*), and fungi (*C. albicans* & *A. flavus*) were chosen for this test concerning the HL ligand and its corresponding complexes. The MIC method was applied, and the results were aggregated in Table 4 and graphed in Fig. 4 (Raman et al., 2003). Two references were screened for comparative evaluation, the first is Ampicillin as the antibacterial reference, and the second is Colitrimazole as antifungal reference. The results point to the superiority of the ligand towards all bacteria which appeared more than the reference. Also, the antifungal screening results are also excellent. The antimicrobial activity of Ni(II) complex comes right after the ligand activity. Unfortunately, the behaviour of rest complexes is ineffective. As reported in various researches (Shah et al., 2016), the existence of functional groups containing nitrogen or sulphur atom enables the chemical compound to interact with electron-deficient centres in biological systems. This is noticed by a distinguish way with the free HL ligand, while this feature was reduced with the complexes. This may refer to the coordination of some functional groups with the metal ions which may cause incapability of such groups for other contributions. Fortunately, the activity of Ni(II) complex is highly significant which is due to the toxic role of nickel atom inside living cells.

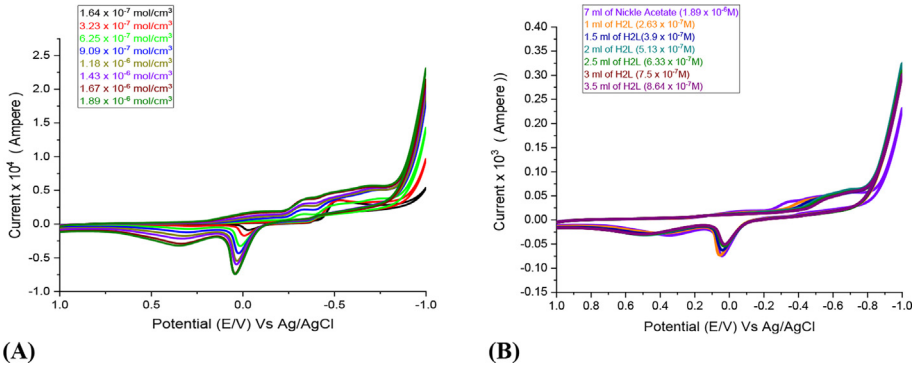

Fig. 3 Influence of different concentrations of Ni(II) in absence of HL (A) and in presence of HL (B) using glassy carbon electrode in 0.1 M KCl at 288.55 K and scan rate 0.1 $V.S^{-1.}$

Table 3 Stability constant for (nickel - HL) complex.

[M] x10^{-3} mol. L^{-1}	[L] × 10^{-4}mol.L^{-1}	(Ep,1/2)M	(Ep,1/2)C	ΔE (V)	J (L/J)	Log βj	ΔG (kJ/mol)
1.84	2.63	−0.205	−0.2141	−0.0091	0.1429	0.3527	−1.949
1.82	3.9	−0.205	−0.2351	−0.0301	0.2142	0.2049	−1.132
1.79	5.13	−0.205	−0.2477	−0.0427	0.2857	0.1943	−1.073
1.77	6.33	−0.205	−0.2553	−0.0503	0.3571	0.2639	−1.458
1.75	7.5	−0.205	−0.2710	−0.0661	0.4285	0.1860	−1.028
1.73	8.64	−0.205	−0.2733	−0.0684	0.5010	0.3376	−1.865

Table 4 The data of antimicrobial activity in terms of MIC (μg/mL).

Compound	*E. coli*	*P. aeuroginosa*	*S. aureus*	*B. subtilis*	*C. Albicans*	*A. flavus*
Ampicillin	125	187	187	93	–	–
Colitrimazole	–	–	–		6	4
1) HL	125	125	125	62	11	6
2) $[Zn(HL)_2(OAc)_2]$	343	337	458	369	73	105
3) $[Ni(L)_2(H_2O)_2]$	165	161	132	109	21	30
4) $[UO_2(L)_2].2H_2O$	338	333	467	366	49	45

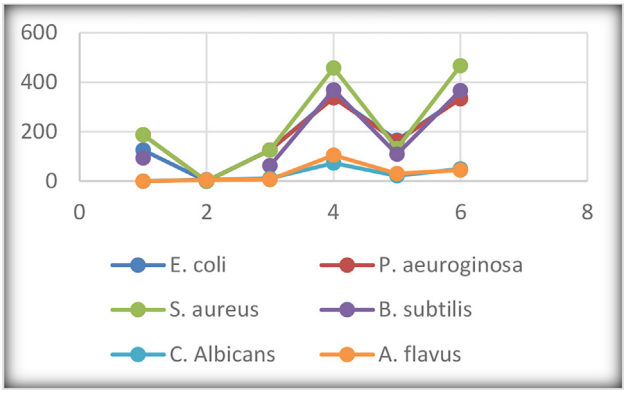

Fig. 4 Antimicrobial activity in terms of MIC (μg/mL).

Table 5 DNA/methyl green colorimetric assay of binding in between.

DNA-active compound	DNA/methyl green (IC_{50}, μg/ml)
1	45.3 ± 2.6
2	78.4 ± 1.6
3	57.9 ± 2.3
4	75.8 ± 2.6

The concentration needed to reduce absorbance of DNA bonded to methyl green to its half value (IC_{50}) was evaluated(mean ± SD, n = 3–5 separate determinations).

B) DNA/methyl green test

Although the bioactivity of newly chemicals are investigated from many scientists, understanding the real mechanism happened inside the living cells is still an area of disagreement. But the best way for choosing the pharmaceutical compound is not area of disagreement between them, they concentrated on the binding activity of such compound with the DNA. The affinity of methyl green to stain the DNA *via* binding at pH = 7 was clearly recorded in a reversible reaction in between (Nagar, 1990). The magnitude of decay in the green color staining the DNA in presence of a tested compound measures the reactivity of such compound in replacing methyl green. This decay was monitored at λ = 630 nm and the concentration of the tested compound causes the absorption reduction to its half value (IC_{50}) was determined for each compound (Table 5). The ligand and $[Ni(L)_2(H_2O)_2]$ complex exhibited significant genotoxicity towards the DNA, particularly the ligand (Ramesh and Maheswaran, 2003). Consequently, controlling the cell-DNA *via* its combination with the compound is the main target to inhibit cell division, resulting induced apoptosis. When the damage of DNA is becoming serious and cannot easily corrected so the cell will death. This damage based on the deterioration of DNA helix due to intercalation of HL ligand with the grooves or through H-bonding. We know the role of aromatic ring in intercalation with DNA, which considered the first part from the ligand that really interacted (Abdel-Rahman et al., 2021). Prospective research is required to determine whether genetic information can improve therapeutic efficacy and safety by assisting with drug selection and dose. Despite the fact that there still many obstacles to overcome, the integration of pharmacogenetics into clinical practice is anticipated to have a substantial impact on health in the upcoming years.

3.8. Quantum-based in-silico tests

A) Pharmit server and MOE module

Here we aimed to examine the extent of effectiveness for binding between the ligand and DNA-polymerase to evaluate the degree of conformity with in-vitro results. Three proteins were chosen from PDB as 1bpy, 5szt and 1zqa (Scheme S5)

for this docking purpose using either the pharmit server (Daina et al., 2017, Fenton et al., 2002; Maiorov and Crippen, 1994) or MOE module (Ver. 2018). Pharmit server, showed a best interaction for the ligand with the pockets of 1bpy and 5szt proteins (Fig. 5). This simulation was ended by searching on analogous drug in MolPort database, a drug with code number MolPort-002–822-252 (Scheme 3) has extent of similarity with HL ligand in its binding with DNA. The Root Mean Square Deviation value (RMSD = 0.266) of the drug is very small which points to the high similarity of such drug with the tested ligand in their biological effectiveness (Maiorov and Crippen, 1994).

Such distinguished behavior of the ligand towards DNA-polymerase was confirmed by MOE-docking (Fig. 6). The ligand interacted perfectly to DG 6(T) residue in 1bpy protein *via* H-donor bond (length 3.3 Å) and the scoring energy value of the docking pose was excellent (S = −6.1512 kcal/mol). While, the allosteric binding with 5szt protein was conducted through various aminio acid residues to produce a pose also with excellent scoring energy (−5.9887 kcal/mol) (Hosny et al., 2020; Katouah et al., 2020).

B) ADME parameters

The absorption, distribution, metabolism and excretion (ADME) are the parameters targeted to investigate the ligand (smaller size) by using Swiss-link. The bioavailability radar (Fig. 7) which exhibited XLOGP3 (lipophilicity), polarization, saturation limit ($sp^3 \geq 0.25$), size, flexibility and solubility indexes on six axis reflects the drug-likeness and physicochemical properties of the ligand. The pink region detects the limits of the optimum values of such indices (Alkhamis et al., 2021). The values of XLOGP3 (2.61), saturation (0.38), size (247.3), polarity (TPSA = 68.51), and flexibility (4) are lower enough to judge on distinguish HL drug-like and physicochemical

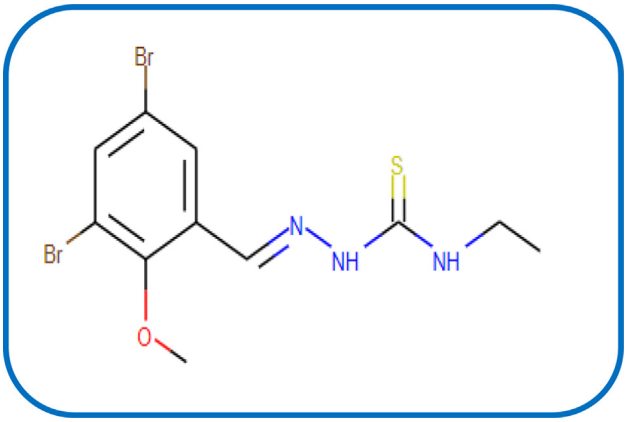

Scheme 3 The structure of MolPort-002–822-252.

properties. The lipophilic feature of the ligand was also supported by Log$P_{o/w}$ (2.74) and Log$S$ (-3.02) values that indicate the lower solubility of HL in polar solvent as water (Alkhamis et al., 2021).

Additionally, the permeability of skin (Log K_p), P-glycoprotein (P-gp) substrate, gastrointestinal tract absorption (GI), brain barrier absorption (BBB), and cytochromes P450 (CYP) were the indices of ligand pharmacokinetics. The behavior of HL ligand towards P-glycoprotein (P-gp) and cytochrome P450 (CYP) enzymes was investigated based on the importance of such protein (P-gp) or these enzymes. The P-gp could protect the nerve cells from xenobiotics although its excretion in tumor cells will resist the anticancer drug action. On the other side, a group of cytochromes which is called *iso*-enzymes (CYP1A2, CYP2C19, CYP2C9, CYP2D6 and CYP3A4) is essential for de-accumulation process (*via* metabolism) of remaining drug inside the cell (Abu-Dief et al., 2021). The HL ligand doesn't play as a substrate of P-

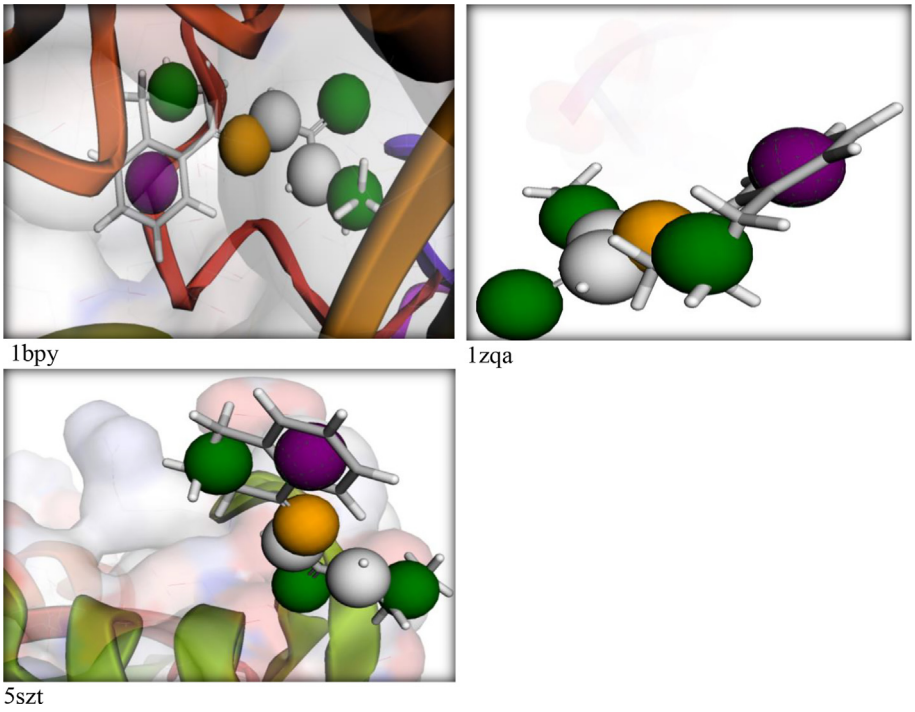

Fig. 5 Pharmit interaction for the HL ligand towards DNA-polymerase proteins.

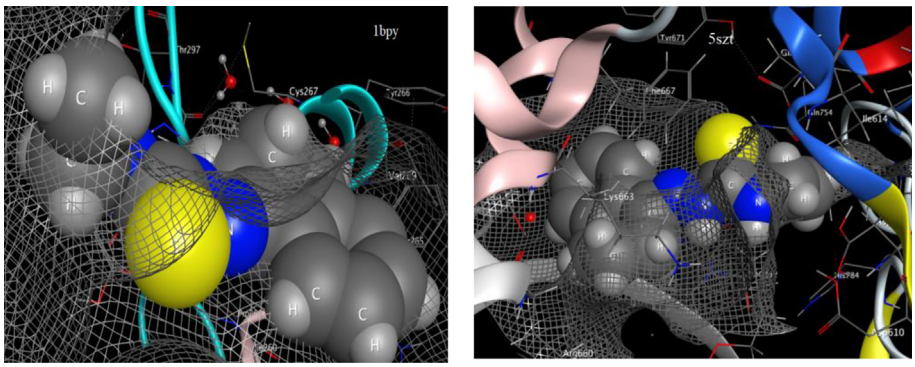

Fig. 6 Effective Interaction of HL with two DNA-polymerase proteins.

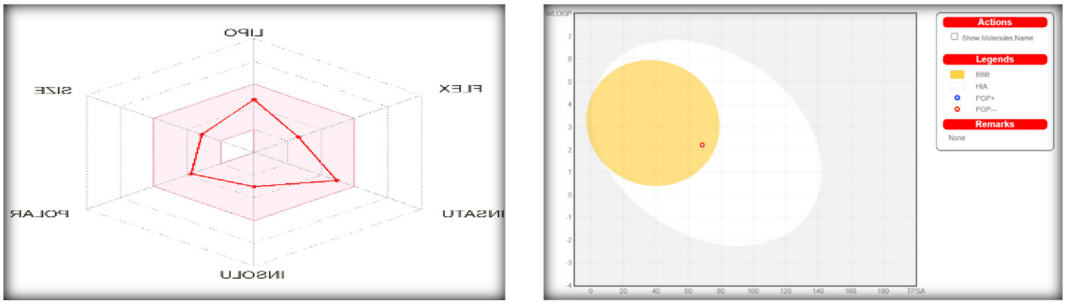

Fig. 7 The bioavailability radar (A) and BOILED-Egg (B) for the ligand via Swiss-ADME study.

gp protein, which is considered favorable for protecting tissues and organisms. Further, the ligand did not inhibit three CYP-enzymes just inhibit CYP1A2 & CYP2C19. So, the drug metabolism process inside the cell did not affected seriously. The log K*p* (-5.96 cm/s) that reflects the relation between lipophilicity and size of the compound, appeared with smaller negative value, indicates the high extent of skin permeability for dug.

Furthermore, the BOILED-Egg image (Fig. 7) which point to a relation between WLOGP and TPSA, indicates the ability of the ligand (red point) to absorb in brain barrier as appeared in yellow region (yolk) (Abu-Dief et al., 2021). While, there is no ability for such compound to absorb in gastrointestinal tract (white zone). Also, the red point reflects the non-substrate function of the ligand towards P-gp (PGP-) protein. The interaction pathway of the ligand inside the living cells (Figure S8) was oriented towards cathepsin L protease; leukocyte elastase protease by 26.7 %, P2X purinoceptor 7 (by homology) ligand-gated ion channel by 20.0 %, and isocitrate dehydrogenase [NADP] cytoplasmic enzyme by 13.3 %. Finally, the interaction of the HL ligand with DNA-polymerase cannot be ignored either from in *vitro* or in *silico* evaluations. This study may be the out of point for other extensive studies aimed at deepening the biological efficacy of the carbothioamide derivative and enriching the rich history of this family of compounds with biological excellence.

4. Conclusion

Three metal ion complexes were derived from thiosemicarbazide derivative by a molar ratio of 1: 2 for metal to ligand. The chemical formulae of all compounds were elucidated by elemental analysis, IR, NMR, UV–Vis, mass spectrum, SEM and EDX and also supported by quantum calculations. The ligand coordinates *via* C(10) = N(11) and C(13) = S(14) groups either as neutral form or as monobasic form. The cyclic voltammetry of Ni^{+2} solution was studied in absence and presence of the ligand to understand the electrochemical changes that happened due to complexation. The high stability constants (β_{ML}) and Gibbs free energies (ΔG) suggest the presence of stable complex in solution. In *vitro* assessments were performed on the new compounds against various microbes as well as methyl green/DNA-binding efficiency. All the results showed exceeding biological efficiency of the ligand moreover appeared superior the antibacterial reference drug. The genotoxicity of the ligand was confirmed *via silico* tests towards the interaction with DNA-polymerase proteins (1bpy, 5szt and 1zqa). Also, the BOILED-Egg indicates the probability of ligand absorption in brain barrier and there is no probability for absorption in gastrointestinal tract. Finally, this study may be the outset point for other extensive studies aimed at deepening the biological efficacy of the carbothioamide derivative and enriching the rich history of this family.

Declaration of Competing Interest

The authors declare that they have no known competing financial interests or personal relationships that could have appeared to influence the work reported in this paper.

Acknowledgement

Princess Nourah bint Abdulrahman University Researchers Supporting Project number (PNURSP2023R22), Princess Nourah bint Abdulrahman University, Riyadh, Saudi Arabia.

Appendix A. Supplementary material

Supplementary data to this article can be found online at https://doi.org/10.1016/j.arabjc.2023.104807.

References

Abdel-Rahman, L.H., Noamaan, M.A., Ahmed, H.E., Adam, M.S.S., 2021. Synthesis, characterization and in vitro pharmacological evaluation of 6,6'-((1E,1'E)-((4-chloro-1,2-phenylene) bis (azaneyl ylidene)) bis(methaneylylidene)) bis (2-ethoxy phenol and its Zr (IV), V(IV), Zn(II) chelates as promising antiproliferative, antimicrobial, antioxidant drug candidates. Bioorg. Chem. 114, 105106.

Abdel-Rhman, M.H., Hussien, M.A., Mahmoud, H.M., Hosny, N.M., 2019. Synthesis, characterization, molecular docking and cytotoxicity studies on N-benzyl-2-isonicotinoylhydrazine-1-carbothioamide and its metal complexes. J. Mol. Struct. 1196, 417–428.

Abu-Dief, A.M., El-khatib, R.M., Aljohani, F.S., Alzahrani, S.O., Mahran, A., Khalifa, M.E., El-Metwaly, N.M., 2021. Synthesis and intensive characterization for novel Zn (II), Pd (II), Cr (III) and VO (II)-Schiff base complexes; DNA-interaction, DFT, drug-likeness and molecular docking studies. J. Mol. Struct., 130693

Abu-Dief, A.M., El-Metwaly, N.M., Alzahrani, S.O., Bawazeer, A.M., Shaaban, S., Adam, M.S.S., 2021. Targeting ctDNA binding and elaborated in-vitro assessments concerning novel Schiff base complexes: synthesis, characterization, DFT and detailed in-silico confirmation. J. Mol. Liq. 322, 114977.

Abumelha, H.M., Al-Fahemi, J.H., Althagafi, I., Bayazeed, A.A., Al-Ahmed, Z.A., Khedr, A.M., El-Metwaly, N.M., 2020. deliberate-characterization for Ni (II)-Schiff Base complexes: promising in-vitro anticancer feature that matched MOE docking-approach. J. Inorg. Organomet. Poly. Mater. 30 (9), 3277–3293.

Alatawi, N.M., Alsharief, H.H., Alharbi, A., Alhasani, M., Attar, R., Khalifa, M.E., Abu-Dief, A.M., El-Metwaly, N.M., 2022. Simulation for the behavior of new Fe (III) and Cr (III)-thiophenyl complexes towards DNA polymerase: synthesis, characterization, eukaryotic DNA and Hartree-Fock computation. Chem. Pap. 76 (6), 3919–3935.

Alaysuy et al., 2022 Alaysuy, O., Abumelha, H.M., Alsoliemy, A., Alharbi, A., Alatawi, N.M., Osman, H.E.M., Zaky, R., El-Metwaly, N.M.,]. Elucidating of new hydrazide-based complexes derived from Pd (II), Cu (II) and Cd (II) ions: studies concerning spectral, DFT, Hirshfeld-crystal, biological screening beside Swiss-ADME verification. J. Mol. Struct. 1259, 132748Hosny et al., 2023Hosny, N.M., Ibrahim, O.A., Belal, A., Hussien, M.A., Abdel-Rhman, M.H., . Synthesis, characterization, DFT, cytotoxicity evaluation and molecular docking of a new carbothioamide ligand and its coordination compounds. Results Chem. 5, 100776.

Al-Hazmi, G.A.A., Abou-Melha, K.S., El-Metwaly, N.M., Althagafi, I., Shaaban, F., Zaky, R., 2020. Green synthesis approach for Fe (III), Cu (II), Zn (II) and Ni (II)-Schiff base complexes, spectral, conformational, MOE-docking and biological studies. Appl. Organomet. Chem. 34 (3).

Alkhamis, K., Alkhatib, F., Alsoliemy, A., Alrefaei, A.F., Katouah, H.A., Osman, H.E., Mersal, G.A., Zaky, R., El-Metwaly, N.M., 2021. Elucidation for coordination features of hydrazide ligand under influence of variable anions in bivalent transition metal salts; green synthesis, biological activity confirmed by in-silico approaches. J. Mol. Struct. 1238, 130410.

Alkhamis, K., Alsoliemy, A., Aljohani, M.M., Alrefaei, A.F., Abumelha, H.M., Mahmoud, M.H., Zaky, R., El-Metwaly, N. M., 2021. Conductometry of nano-sized zinc sulfate; synthesis and characterization of new hydrazone complexes: conformational and in-vitro assay. J. Mol. Liq. 340, 117167.

Alkhamis, K., Alsoliemy, A., Aljohani, M.M., Alrefaei, A.F., Abumelha, H.M., Mahmoud, M.H., Zaky, R., El-Metwaly, N. M., 2021. Conductometry of nano-sized zinc sulfate; synthesis and characterization of new hydrazone complexes: conformational and in-vitro assay. J. Mol. Liq. 340, 117167.

Alkhamis, K., Alatawi, N.M., Alsoliemy, A., Qurban, J., Alharbi, A., Khalifa, M.E., Zaky, R., El-Metwaly, N.M., 2022. Synthesis and investigation of bivalent thiosemicarbazone complexes: conformational analysis, methyl green DNA binding and in-silico studies. Arab. J. Sci. Eng. 1–18.

Almehmadi, S.J., Alharbi, A., Abualnaja, M.M., Alkhamis, K., Alhasani, M., Abdel-Hafez, S.H., Zaky, R., El-Metwaly, N.M., 2022. Solvent free synthesis, characterization, DFT, cyclic voltammetry and biological assay of Cu (II), Hg (II) and UO2 (II)–Schiff base complexes. Arb. J. Chem 15 (2), 103586.

Al-Qahtani, S.D., Alsoliemy, A., Almehmadi, S.J., Alkhamis, K., Alrefaei, A.F., Zaky, R., El-Metwaly, N.M., 2021. Green synthesis for new Co (II), Ni (II), Cu (II) and Cd (II) hydrazone-based complexes; characterization, biological activity and electrical conductance of nano-sized copper sulphate. J. Mol. Struct. 1244, 131238.

Alzahrani, S., Morad, M., Bayazeed, A., Aljohani, M.M., Alkhatib, F., Shah, R., Katouah, H., Abumelha, H.M., Althagafi, I., Zaky, R., El-Metwaly, N.M., 2020. Ball milling approach to prepare new Cd (II) and Zn (II) complexes; characterization, crystal packing, cyclic voltammetry and MOE-docking agrees with biological assay. J. Mol. Struct. 1218, 128473.

Antony, R., David, S.T., Saravanan, K., Karuppasamy, K., Balakumar, S., 2013. Synthesis, spectrochemical characterisation and catalytic activity of transition metal complexes derived from Schiff base modified chitosan. Spectrochim. Acta A 103, 423–430.

Burres, N., Frigo, A., Rasmussen, R., McAlpine, J., 1992. A colorimetric microassay for the detection of agents that interact with DNA. J Nat Prod 55, 1582–1587.

Casas, J.S., García-Tasende, M.S., Sordo, J., 2000. Main group metal complexes of semicarbazones and thiosemicarbazones. A structural review. Coordination Chem. Rev. 209 (1), 197–261.

Cotton, F.A., Wilkinson, G., Murillo, C.A., Bochmann, M., 2003. Advanced Inorganic Chemistry. John Wiley & Sons Inc, pp. 1–171.

Daina et al., 2017Daina, A., Michielin, O., Zoete, V., 0]. Sci. Rep. 7, 42717Fenton et al., 2002Fenton, R.R., Gauci, R., Junk, P.C., Lindoy, L.F., Luckay, R.C., Meehan, G.V., Price, J.R., Turner, P., Wei, G., . Macrocyclic ligand design. Structure–function relationships involving the interaction of pyridinyl-containing, mixed oxygen–nitrogen donor macrocycles with cobalt (II), nickel (II), copper (II), zinc (II), cadmium (II), silver (I) and lead (II). J. Chem. Soc. Dalton Trans. 10, 2185–2193.

El-Asmy et al., 2015El-Asmy, A., Jeragh, B., Ali, M., 1]. Spectral, thermal, molecularmodeling and biological studies on monoand-binuclear complexes derived from oxalobis(2,3-butanedionehydrazone). Chem. Cent. J. 9, 1–12Hosny et al., 2019Hosny, N.M., Hassan, N.Y., Mahmoud, H.M., Abdel-Rhman, M.H., . Synthesis, characterization and cytotoxicity of new 2-isonicotinoyl-N-phenyl-hydrazine-1-carbothioamide and its metal complexes. Appl. Organomet. Chem. 33 (8), e4998.

Frisch, M.J., Trucks, G.W., Pople, J.A., 2009. Gaussian 09, Revision B.2, Gaussian, Inc., Pittsburgh, PA.

Hehre, W.J., Radom, L., Schlyer, P.V.R., Pople, J.A., 1986. Ab Initio Molecular Orbital Theory. Wiley, New York.

Hosny, N.M., Hussien, M.A., Motawa, R., Belal, A., Abdel-Rhman, M.H., 2020. Synthesis, Spectral, Modeling, Docking and Cytotoxicity Studies on 2-(2-aminobenzoyl)-N-ethylhydrazine-1-carbothioamide and its divalent metal complexes. Appl. Organomet. Chem. 34 (11), e5922.

Katouah, H., Sayqal, A., Al-Solimy, A.M., Abumelha, H.M., Shah, R., Alkhatib, F., Alzahrani, S., Zaky, R., El-Metwaly, N.M., 2020. Facile synthesis and deliberate characterization for new hydrazide complexes; cyclic voltammetry, crystal packing, eukaryotic DNA degradation and in-silico studies. J. Mol. Liq. 320, 114380.

Khandar, A.A., Azar, Z.M., Eskandani, M., Hubschle, C.B., Smaalen, S., Shaabani, B., Omidi, Y., 2019. Cadmium(II) complexes of a hydrazone ligand: Synthesis, characterization, DNA binding, cyto- and genotoxicity studies. Polyhedron 171, 237–248.

Leovac, V.M., Novaković, S.B., Bogdanović, G.A., Joksović, M.D., Szécsényi, K.M., Češljević, V.I., 2007. Transition metal complexes with thiosemicarbazide-based ligands. Part LVI: Nickel(II) complex with 1,3-diphenylpyrazole-4-carboxaldehyde thiosemicarbazone and unusually deformed coordination geometry. Polyhedron 26 (14), 3783–3792.

Lever, A.B.P., 1968. Inorganic Electronic Spectroscopy. Elsevier, Amsterdam, pp. 1–863.

Liberta and West, 1992Liberta, A.E., West, D.X., 9]. Antifungal and antitumor activity of heterocyclic thiosemicarbazones and their metal complexes: current status. Biometals 5 (2), 121–126Li et al., 2017Li, Q., Zhou, P., Yan, H.J., . Improved thermal lattice Boltzmann model for simulation of liquid-vapor phase change. Phys. Rev. E 96, 063303.

Maiorov, V.N., Crippen, G.M., 1994. Significance of root-mean-square deviation in comparing three-dimensional structures of globular proteins. J. Mol. Biol. 235 (2), 625–634.

McGlynn, S., Smith, J., Neely, W., 1961. Electronic structure, spectra, and magnetic properties of oxycations. III. Ligation effects on the infrared spectrum of the uranyl ion. J. Chem. Phys. 35 (1), 105–116.

Miminoshvili, E.B., 2009. Metal hydrazide complexes. J. Struct. Chem. 50 (1), 168–175.

Modeling and Simulation Solutions for Chemicals and Materials Research, Materials Studio (Version 5.0), 2009. Accelrys software Inc., San Diego, USA. Available online at: http://www.accelrys.com.

Morgan, S.M., El-Sonbati, A.Z., Eissa, H.R., 2017. Geometrical structures, thermal properties and spectroscopic studies of Schiff base complexes: Correlation between ionic radius of metal complexes and DNA binding. J. Mol. Liq. 240, 752–776.

Nagar, R., 1990. Syntheses, characterization, and microbial activity of some transition metal complexes involving potentially active O and N donor heterocyclic ligands. J Inorg Biochem 40, 349–356.

Nakamoto, K., 1970. Infrared Spectra of Inorganic and Coordination Compounds. Wiley, New York, pp. 1–338.

Netalkar, P.P., Netalkar, S.P., Revankar, V.K., 2015. Transition metal complexes of thiosemicarbazone: Synthesis, structures and invitro antimicrobial studies. Polyhedron 100, 215–222.

Pelosi, G., 2010. Thiosemicarbazone metal complexes: from structure to activity. Open Crystallogr. J. 3, 16–28.

Pelosi, G., Bisceglie, F., Bignami, F., Ronzi, P., Schiavone, P., 2010. Maria Carla Re, Claudio Casoli, Elisabetta Pilotti, Antiretroviral activity of thiosemicarbazone metal complexes. J. Med. Chem. 53 (24), 8765.

Qurban, J., Al-Qahtani, S.D., Alsoliemy, A., Alharbi, A., Alkhamis, K., Al-nami, S.Y., Zaky, R., El-Metwaly, N.M., 2022. Tailoring of new Ni(II), Hg(II) and UO_2(II)–hydrazide complexes: characterization, studies in-vitro and in-silico as well as the Hartree-Fock modeling. J. Saudi Chem. Soc. 26, (3) 101477.

Raman, N., Muthuraj, V., Ravichandran, S., Kulandaisamy, A., 2003. Synthesis, characterization and electrochemical behaviour of Cu (II), Co(II), Ni(II) and Zn(II) complexes derived from acetylacetone and p-anisidine and their antimicrobial activity. Proc. Indian Acad. Sci. 115, 161–167.

Ramesh, R., Maheswaran, S.J., 2003. Synthesis, spectra, dioxygen affinity and antifungal activity of Ru(III) Schiff base complexes. J. Inorg. Biochem. 96, 457–462.

Shah, R.K., Abou-Melha, K.S., Saad, F.A., Yousef, T., Al-Hazmi, G. A., Elghalban, M.G., Khedr, A.M., El-Metwaly, N.M., 2016. Elaborated studies on nano-sized homo-binuclear Mn (II), Fe (III), Co (II), Ni (II), and Cu (II) complexes derived from N_2O_2 Schiff base, thermal, molecular modeling, drug-likeness, and spectral. J. Therm. Anal. Calorim. 123 (1), 731–743.

Sumrra, S.H., Habiba, U., Zafar, W., Imran, M., Chohan, Z.H., 2020. A review on the efficacy and medicinal applications of metal-based triazole derivatives. J. Coord. Chem. 73 (20–22), 2838–2877.

Vogel, A.I., 1989. Quantitative Inorganic Analysis. Longmans, London.

West, D.X., Padhye, S.B., Sonawane, P.B., 1990. Structural and physical correlations in the biological properties of transition metal heterocyclic thiosemicarbazone and S-alkyldithiocarbazate complexes. Struct. Bonding 76, 1–50.

West et al., 1993West, D.X., Liberta, A.E., Padhye, S.B., 7]. Thiosemicarbazone complexes of copper (II): structural and biological studies. Coordination Chem. Rev. 123 (1–2), 49–71Hosny et al., 2018Hosny, N.M., Mahmoud, H.M., Abdel-Rhman, M.H., . Spectral, optical, and cytotoxicity studies on N-(2-isonicotinoylhydrazine-carbonothioyl)benzamide and its metal complexes. Heteroatom Chem. 29 (2), e21415.